Available online at www.sciencedirect.com
ScienceDirect
Journal of Solid State Chemistry 180 (2007) 1595–1600
JOURNAL OF SOLID STATE CHEMISTRY
www.elsevier.com/locate/jssc

$Pr_4B_{10}O_{21}$: A new composition of rare-earth borates by high-pressure/high-temperature synthesis

Almut Haberer, Gunter Heymann, Hubert Huppertz*

Department Chemie und Biochemie, Ludwig–Maximilians–Universität München, Butenandtstrasse 5–13, D–81377 München, Germany

Received 14 January 2007; received in revised form 23 February 2007; accepted 26 February 2007
Available online 12 March 2007

Abstract

High-pressure chemistry led to the synthesis of the rare-earth borate $Pr_4B_{10}O_{21}$ using a Walker-type multianvil apparatus at 3.5 GPa and 1050 °C. The tetra-praseodymium(III)-decaborate crystallizes monoclinicly with four formula units in the space group $P2_1/n$ and lattice parameters of $a = 710.2(2)$, $b = 1948.8(4)$, $c = 951.6(2)$ pm, and $\beta = 93.27(3)°$. The boron–oxygen network consists of $[BO_4]^{5-}$ tetrahedra and $[BO_3]^{3-}$ groups; however, the $[BO_4]^{5-}$ groups represent the major part (80%) due to the high-pressure conditions during the synthesis. The praseodymium ions are coordinated by 10 and 12 oxygen atoms. Along with a detailed description of the crystal structure, temperature programmed X-ray powder diffraction data are shown, demonstrating the metastable character of this compound.

Keywords: High-pressure; Multianvil; Crystal structure; Borate

1. Introduction

Over the past years, we have investigated the synthetic possibilities in oxoborate chemistry under high-pressure conditions. Next to the synthesis of new interesting high-pressure polymorphs like β-MB_4O_7 (M = Ca, Zn, Hg) [1–3], χ–$RE BO_3$ (RE = Dy, Er) [4], ν–$DyBO_3$ [5], γ–$RE(BO_2)_3$ (RE = La–Nd) [6], δ–$La(BO_2)_3$ [7], and δ–BiB_3O_6 [8], we have focussed on the synthesis of new compositions, which are not attainable at ambient pressure conditions. For example, in the glass forming ternary systems Sn–B–O or Hf–B–O the compounds β–SnB_4O_7 [9] and β–HfB_2O_5 [10] were synthesized by pressure-induced crystallization. In the field of rare-earth borates, it was possible to synthesize the compounds $RE_4B_6O_{15}$ (RE-Dy, Ho) [11–13], α–$RE_2B_4O_9$ (RE = Sm–Ho) [14–16], β–$RE_2B_4O_9$ (RE = Dy, Gd) [17,18], and $RE_3B_5O_{12}$ (RE = Tm–Lu) [19] at pressures of 8, 7.5–10, 3–5, and 10 GPa, respectively. As a common trend in these metastable high-pressure oxoborates, the boron atoms favour the fourfold coordination with increasing pressure. At conditions exceeding 7 GPa, we could only find tetrahedrally coordinated boron atoms. Additionally, we observed that these tetrahedra, which are normally linked via common corners, can share common edges to realize denser structures (α–$RE_2B_4O_9$ (RE = Sm–Ho) [14–16] and $RE_4B_6O_{15}$ (RE = Dy, Ho) [11–13]). Furthermore, the rare-earth ions show increased coordination numbers (CN), and also the CN of the oxygen atoms can be partially enhanced from two (O^2) to three (O^3).

With the high-pressure/high-temperature synthesis of $Pr_4B_{10}O_{21}$, we now add a new composition to the existing rare-earth oxoborates. For an overview of existing rare-earth oxoborates see Ref. [12]. In the following, we describe the synthesis, the single-crystal structure, IR spectroscopic investigations, and the thermal behavior of $Pr_4B_{10}O_{21}$.

2. Experimental part

According to Eq. (1), $Pr_4B_{10}O_{21}$ was prepared via a high-temperature/high-pressure synthesis from Pr_6O_{11} (Auer–Remy K.-G., Hamburg, Germany, >99.9%) and

*Corresponding author. Fax: +49 89 218077806.
E-mail address: huh@cup.uni-muenchen.de (H. Huppertz).

0022-4596/$ - see front matter © 2007 Elsevier Inc. All rights reserved.
doi:10.1016/j.jssc.2007.02.021

B_2O_3 (Strem Chemicals, Newburyport, USA, >99.9%):

$$2\ Pr_6O_{11} + 15\ B_2O_3 \xrightarrow[3.5\ GPa]{1050\ ^\circ C} 3\ Pr_4B_{10}O_{21} + 2\ O_2. \quad (1)$$

A stoichiometric mixture of the oxides (ca. 50 mg) was ground and placed into a boron nitride crucible of an 18/11-assembly, which was compressed up to 3.5 GPa during 90 min, using a multianvil apparatus. Details of preparing the assembly can be found in Refs. [20–24]. The sample was heated to 1050 °C in 20 min. After 5 min at 1050 °C, the sample was cooled down to 450 °C in 30 min, followed by quenching to room temperature. The decompression of the assembly required 5 h. The recovered experimental octahedron was opened and the sample carefully separated from the surrounding boron nitride crucible, yielding the light-green, crystalline, nearly phase pure compound $Pr_4B_{10}O_{21}$.

Table 1
Crystal data and structure refinement for $Pr_4B_{10}O_{21}$

Empirical formula	$Pr_4B_{10}O_{21}$
Molar mass/g mol^{-1}	1007.74
Crystal system	Monoclinic
Space group	$P2_1/n$ (No.14)
Powder diffractometer	STOE STADI P
Radiation	Cu-$K\alpha_1$ ($\lambda = 154.06$ pm)
Powder–diffraction data	
a/pm	711.2(2)
b/pm	1951.9(3)
c/pm	952.1(2)
β/°	93.20(2)
Volume/Å^3	1319.7(3)
Single-crystal diffractometer	STOE–IPDS
Radiation	Mo-$K\alpha$ ($\lambda = 71.073$ pm)
Single-crystal data	
a/pm	710.2(2)
b/pm	1948.8(4)
c/pm	951.6(2)
β/°	93.27(3)
Volume/Å^3	1314.9(5)
Formula units per cell	$Z = 4$
Temperature/K	293(2)
Calculated density/g cm^{-3}	5.090
Crystal size/mm^3	$0.082 \times 0.072 \times 0.045$
Detector distance/mm	40.0
Irradiation/exposure/min	10
Number of exposures	180
Absorption coefficient/mm^{-1}	14.708
F(000)	1816
θ range/°	3.49 to 30.00
Range in hkl	$\pm 9, \pm 27, \pm 13$
Total no. reflections	13476
Independent reflections	3808 ($R_{int} = 0.0326$)
Reflections with $I > 2\sigma(I)$	3143 ($R_\sigma = 0.0249$)
Data/parameters	3808/317
Absorption correction	Numerical (HABITUS [25])
Transm. ratio (min/max)	0.3798/0.5280
Goodness-of-fit (F^2)	0.981
Final R indices ($I > 2\sigma(I)$)	$R_1 = 0.0219$
	$wR_2 = 0.0540$
R indices (all data)	$R_1 = 0.0302$
	$wR_2 = 0.0558$
Extinction coefficient	0.00130(8)
Larg. diff. peak and hole/e Å^{-3}	1.52/−1.33

3. Crystal structure analysis

Small single crystals of $Pr_4B_{10}O_{21}$ were isolated by mechanical fragmentation and examined by Laue photographs on a Buerger precession camera. Single-crystal intensity data of $Pr_4B_{10}O_{21}$ were measured with a STOE-IPDS [Mo-$K\alpha$ radiation (71.073 pm)]. The data were subjected to a numerical absorption correction (Habitus [25]). According to the systematic extinctions $h0l$ with $h + l \neq 2n$, $0k0$ with $k \neq 2n$, $h00$ with $h \neq 2n$, and $00l$ with $l \neq 2n$, the monoclinic space group $P2_1/n$ (Nr. 14) was derived. The structure solution and the parameter refinement (full-matrix least-squares against F^2) were carried out via direct methods, making use of the SHELX–97 software suite [26]. The final difference Fourier syntheses revealed no significant residual peaks. All relevant crystallographic data and details of the data collection are in Table 1. The positional parameters and interatomic distances are listed in Tables 2–4. Additional information of the crystal

Table 2
Atomic coordinates (Wyckoff site 4e for all atoms) and isotropic equivalent displacement parameters (U_{eq}/Å^2) for $Pr_4B_{10}O_{21}$ (space group: $P2_1/n$)

Atom	x	y	z	U_{eq}
Pr1	0.37346(3)	0.19987(2)	0.83901(2)	0.00979(6)
Pr2	0.89592(3)	0.29474(2)	0.82460(2)	0.00943(7)
Pr3	0.35865(3)	0.41705(1)	0.83722(2)	0.00849(6)
Pr4	0.84521(3)	0.08081(1)	0.84440(2)	0.00927(7)
O1	0.2975(4)	0.5180(2)	0.9721(3)	0.0083(5)
O2	0.6293(4)	0.1588(2)	0.0183(3)	0.0093(5)
O3	0.3520(4)	0.1187(2)	0.6331(3)	0.0080(5)
O4	0.1273(4)	0.3429(2)	0.0180(3)	0.0088(5)
O5	0.8732(4)	0.3857(2)	0.6440(3)	0.0084(5)
O6	0.0520(4)	0.1778(2)	0.8969(3)	0.0099(5)
O7	0.1641(4)	0.0417(2)	0.7727(3)	0.0078(5)
O8	0.4543(4)	0.0718(2)	0.9146(3)	0.0091(5)
O9	0.5734(4)	0.3129(2)	0.9052(3)	0.0109(5)
O10	0.9560(4)	0.4288(2)	0.9141(3)	0.0090(5)
O11	0.6933(4)	0.1880(2)	0.7579(3)	0.0085(5)
O12	0.2156(4)	0.3159(2)	0.7641(3)	0.0091(5)
O13	0.1349(4)	0.4519(2)	0.1397(3)	0.0094(5)
O14	0.8911(4)	0.2346(2)	0.0785(3)	0.0102(5)
O15	0.3298(4)	0.5398(2)	0.2247(3)	0.0082(5)
O16	0.5373(4)	0.3749(2)	0.6262(3)	0.0104(5)
O17	0.0141(4)	0.1134(2)	0.5991(3)	0.0102(5)
O18	0.6868(4)	0.4740(2)	0.5260(3)	0.0093(5)
O19	0.7262(4)	0.2697(2)	0.5814(3)	0.0115(5)
O20	0.0886(4)	0.2296(2)	0.6396(3)	0.0119(5)
O21	0.1583(4)	0.4521(2)	0.6277(3)	0.0110(5)
B1	0.0155(6)	0.4058(2)	0.0557(4)	0.0077(7)
B2	0.8060(6)	0.4786(2)	0.8967(4)	0.0081(7)
B3	0.0251(6)	0.4055(2)	0.5560(4)	0.0076(7)
B4	0.2968(6)	0.0239(2)	0.8986(4)	0.0068(7)
B5	0.6982(6)	0.4230(2)	0.6386(4)	0.0079(7)
B6	0.5454(6)	0.3126(2)	0.5460(5)	0.0096(8)
B7	0.7089(6)	0.2070(2)	0.1204(5)	0.0092(7)
B8	0.1941(6)	0.0715(2)	0.6332(4)	0.0069(7)
B9	0.5637(6)	0.3224(2)	0.0456(5)	0.0099(7)
B10	0.6814(6)	0.2028(2)	0.6201(5)	0.0103(7)

U_{eq} is defined as one-third of the trace of the orthogonalized U_{ij} tensor.

Table 3
Interatomic praseodymium–oxygen distances (d/pm), calculated with the single-crystal lattice parameters of $Pr_4B_{10}O_{21}$ (standard deviations in parentheses)

Pr1–O6	241.7(3)	Pr2–O12	241.0(3)	Pr3–O12	230.6(3)	Pr4–O6	242.8(3)
Pr1–O11	245.1(3)	Pr2–O5	246.7(3)	Pr3–O1	240.2(3)	Pr4–O18a	243.7(3)
Pr1–O3	251.6(3)	Pr2–O9	248.2(3)	Pr3–O15	247.0(3)	Pr4–O13	247.0(3)
Pr1–O2	254.9(3)	Pr2–O4	257.3(3)	Pr3–O21	247.8(3)	Pr4–O11	247.1(3)
Pr1–O12	260.6(3)	Pr2–O11	258.7(3)	Pr3–O16	257.0(3)	Pr4–O7	252.0(3)
Pr1–O8	265.2(3)	Pr2–O19	259.4(3)	Pr3–O9	259.9(3)	Pr4–O15	261.2(3)
Pr1–O19	265.4(3)	Pr2–O6	261.0(3)	Pr3–O7	264.7(3)	Pr4–O17	275.9(3)
Pr1–O9	267.6(3)	Pr2–O20	261.9(3)	Pr3–O17	273.3(3)	Pr4–O2	277.3(3)
Pr1–O20	275.6(3)	Pr2–O14	268.8(3)	Pr3–O4	284.0(3)	Pr4–O8	289.8(3)
Pr1–O14	279.8(3)	Pr2–O10	277.4(3)	Pr3–O10	300.1(3)	Pr4–O16	306.3(3)
						Pr4–O18b	308.8(3)
						Pr4–O21	313.8(3)
	∅ 260.7		∅ 258.0		∅ 260.5		∅ 272.1

Table 4
Interatomic boron–oxygen distances (d/pm), calculated with the single crystal lattice parameters of $Pr_4B_{10}O_{21}$ (standard deviations in parentheses)

B1–O13	144.6(5)	B2–O10	144.3(5)
B1–O10	145.9(5)	B2–O13	146.4(5)
B1–O3	148.9(5)	B2–O1	148.7(5)
B1–O4	151.4(5)	B2–O15	150.6(5)
	Ø 147.1		Ø 147.5
B3–O21	145.3(5)	B4–O8	145.8(5)
B3–O5	145.6(5)	B4–O21	146.1(5)
B3–O8	147.7(5)	B4–O18	147.9(5)
B3–O2	150.8(5)	B4–O7	152.1(4)
	Ø 147.4		Ø 148.0
B5–O5	143.8(5)	B6–O6	143.5(5)
B5–O18	146.1(5)	B6–O16	143.7(5)
B5–O16	147.9(5)	B6–O14	147.6(5)
B5–O15	151.1(5)	B6–O19	155.3(5)
	Ø 147.2		Ø 147.5
B7–O12	143.7(5)	B8–O1	144.9(5)
B7–O2	144.3(5)	B8–O3	145.0(5)
B7–O14	147.7(5)	B8–O7	147.5(5)
B7–O20	152.0(5)	B8–O17	153.5(5)
	Ø 146.9		Ø 147.7
B9–O9	135.4(5)	B10–O11	134.0(5)
B9–O20	135.7(3)	B10–O4	135.7(5)
B9–O17	140.2(5)	B10–O19	139.7(5)
	Ø 137.1		Ø 136.5

structure investigation may be obtained from the Fachinformationszentrum Karlsruhe, 76344 Eggenstein Leopoldshafen, Germany (fax: +49 7247 808 666; e-mail: crystdata@fiz–karlsruhe.de), on quoting the depository number CSD–417553.

The powder diffraction pattern was obtained in transmission geometry from a flat sample of $Pr_4B_{10}O_{21}$, using a STOE STADI P powder diffractometer with monochromatized Cu-$K\alpha_1$ radiation. The diffraction pattern was indexed with the program ITO [27] on the basis of a monoclinic unit cell. The calculation of the lattice parameters (Table 1) was founded on least-square fits of the powder data. The correct indexing of the patterns of $Pr_4B_{10}O_{21}$ was confirmed by intensity calculations, employing the atomic positions of the structure refinement [28].

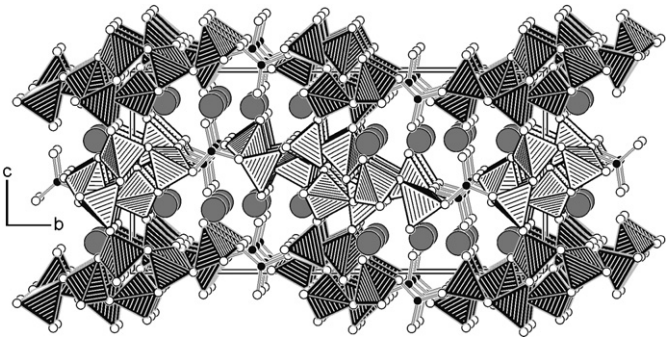

Fig. 1. Crystal structure of $Pr_4B_{10}O_{21}$, view along [$\bar{1}$00].

The lattice parameters, deduced from the powder data and the single-crystal data, matched well.

4. Results and discussion

Fig. 1 shows the crystal structure of $Pr_4B_{10}O_{21}$ along [100]. The structure is composed of trigonal $[BO_3]^{3-}$ and tetrahedral $[BO_4]^{5-}$ groups, which are linked to a highly condensed network. For a better understanding of the structure, the $[BO_4]^{5-}$ tetrahedra in Fig. 1 are partitioned in corrugated layers of black tetrahedra and light tetrahedra. These layers are connected via corner sharing $[BO_4]^{5-}$ tetrahedra. Fig. 2 clearly reveals the linkage of $[BO_3]^{3-}$ and $[BO_4]^{5-}$ groups inside the layer. In the bottom of Fig. 2, the two building blocks of this layer appear. The first building block (Fig. 2, bottom left) consists of 10 tetrahedra, forming a central four-membered ring and two three-membered rings. Additionally, four $[BO_4]^{5-}$ tetrahedra are added to the outer rings (two on each side). The second building block (Fig. 2, bottom right) is built up from six $[BO_4]^{5-}$ tetrahedra and four $[BO_3]^{3-}$ groups. Similar to the first building block, the $[BO_4]^{5-}$ tetrahedra form a central four-membered ring with two three-membered rings on either side. In contrast, the four $[BO_4]^{5-}$ tetrahedra added to the outer rings in the first building block are substituted by four trigonal $[BO_3]^{3-}$ groups. The linkage of these two

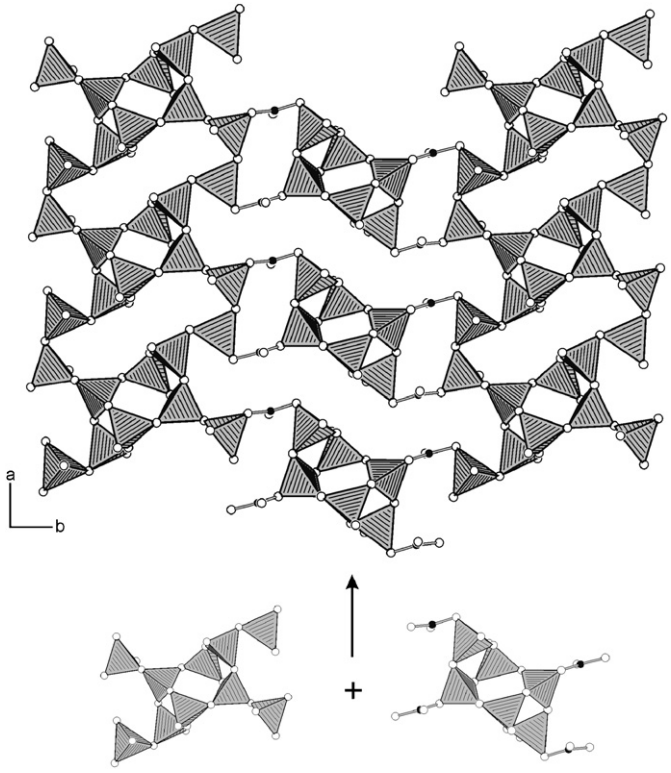

Fig. 2. Crystal structure of $Pr_4B_{10}O_{21}$, showing a layer of $[BO_4]^{5-}$ tetrahedra and $[BO_3]^{3-}$ groups perpendicular to [001].

building blocks via the outer $[BO_4]^{5-}$ tetrahedra and $[BO_3]^{3-}$ groups constructs the entire layer.

$Pr_4B_{10}O_{21}$ contains 10 crystallographically distinguishable boron atoms. Eight of them possess a tetrahedral and two a trigonal oxygen coordination sphere. Inside the tetrahedra, the B–O distances vary between 143 and 156 pm (Table 4) with a mean value of 147.5 pm, which corresponds well with the known average value of 147.6 pm for boron–oxygen bond lengths in $[BO_4]^{5-}$ tetrahedra [29,30]. The trigonal groups show boron–oxygen distances of 134–140 pm with a mean value of 136.8 pm, which agrees with the known value of 137.0 pm for oxoborates within $[BO_3]^{3-}$ groups [30,31]. The angles O–B–O inside the $[BO_4]^{5-}$ groups range between 97.3° and 117.2° at a mean value of 109.4°.The angles inside the trigonal $[BO_3]^{3-}$ groups exhibit values of 116.9–124.0° at a mean value of 120°.

The Pr^{3+} ions are positioned in channels between the layers (Fig. 1). Fig. 3 provides a view of the coordination spheres of the four Pr^{3+} ions in $Pr_4B_{10}O_{21}$. The ions Pr1, Pr2, and Pr3 are coordinated by 10 oxygen atoms in the ranges 242–280, 241–278, and 231–301 pm, respectively (Table 3). Theses values fit well to the coordination polyhedra of the Pr^{3+} ion in the praseodymium *meta*-borate $Pr(BO_2)_3$, where the Pr^{3+} ions are also coordinated by 10 oxygen atoms with Pr–O distances ranging from 239 to 281 pm [32]. The fourth praseodymium ion (Pr4) in $Pr_4B_{10}O_{21}$ exhibits a larger CN of 12 with Pr–O distances of 243–314 pm. A calculation of the bond–valence sums

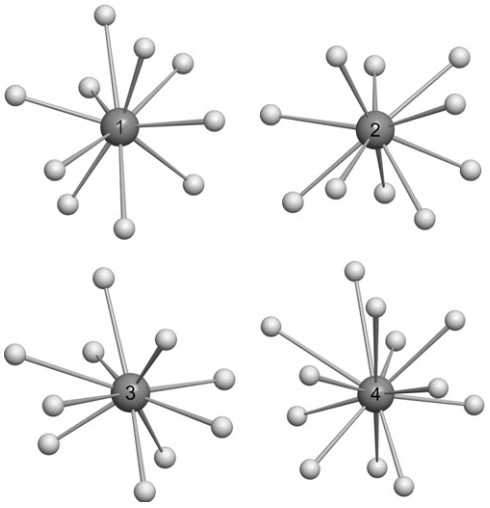

Fig. 3. Coordination spheres of the praseodymium ions in $Pr_4B_{10}O_{21}$.

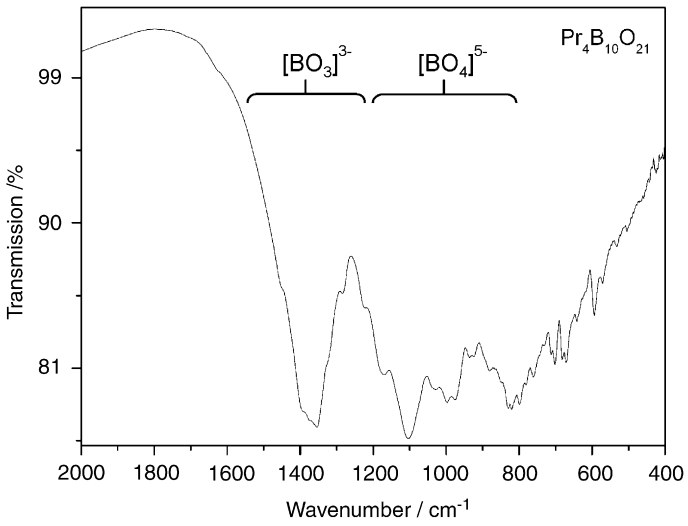

Fig. 4. IR spectrum of $Pr_4B_{10}O_{21}$.

[33,34] for the praseodymium ions in $Pr_4B_{10}O_{21}$ revealed values of +2.96 (Pr1), +3.14 (Pr2), +3.23 (Pr3), and +3.07 (Pr4), which fit well to the formal ionic charges of the atoms.

4.1. Infrared spectroscopy of $Pr_4B_{10}O_{21}$

The infrared spectrum of $Pr_4B_{10}O_{21}$ was recorded on a Bruker IFS66/v spectrometer, scanning a range from 400 to 4000 cm^{-1}. The samples were thoroughly mixed with dried KBr (5 mg sample, 500 mg KBr) in a glove box under dried argon atmosphere. Fig. 4 shows the spectral region between 400 and 2000 cm^{-1}. The presence of $[BO_4]^{5-}$ groups next to $[BO_3]^{3-}$ groups could be confirmed by this investigation. The absorption peaks between 790 and 1200 cm^{-1} are typical of the tetrahedral borate group $[BO_4]^{5-}$ as in π-$GdBO_3$, π-YBO_3, or $TaBO_4$ [35–37]. The absorptions between 1300 and 1450, around 1200 and below 790 cm^{-1}, are characteristic of triangular $[BO_3]^{3-}$

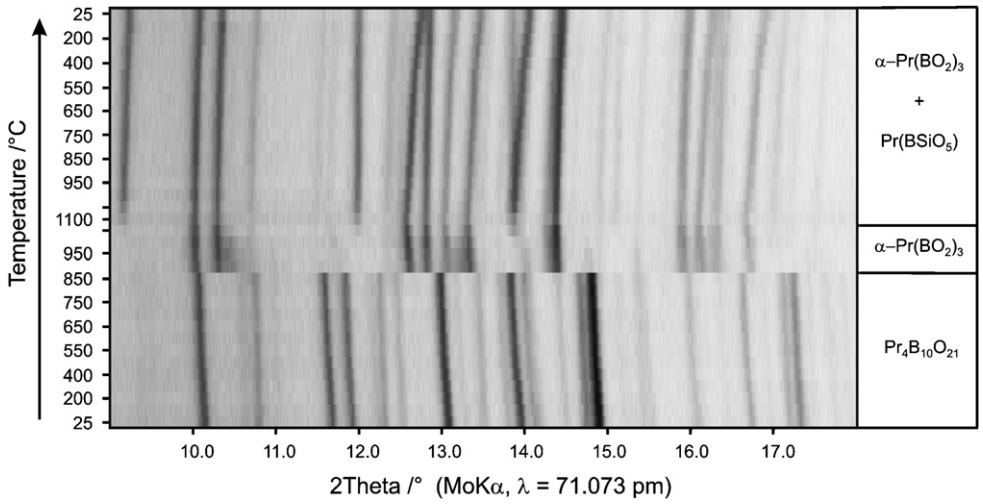

Fig. 5. Temperature programmed X-ray powder diffraction patterns, following the decomposition of the metastable high-pressure phase $Pr_4B_{10}O_{21}$ into the monoclinic normal-pressure form α-$Pr(BO_2)_3$. At higher temperatures, a side reaction with the mark capillary occurs.

groups as in λ-$LaBO_3$ [38], H-$LaBO_3$ [39], or EuB_2O_4 [40]. Due to the fact that eight different tetrahedra and two trigonal groups occur in the structure of $Pr_4B_{10}O_{21}$, a more detailed assignment of the bands is not possible.

4.2. Thermal behavior of $Pr_4B_{10}O_{21}$

Temperature programmed X-ray powder diffraction experiments were performed on a STOE STADI P powder diffractometer [Mo-$K\alpha$ radiation (71.073 pm)] with a computer controlled STOE furnace: The sample was enclosed in a quartz capillary and heated from room temperature to 500 °C in 100 °C steps, and from 500 to 1100 °C in 50 °C steps. Afterwards, the sample was cooled down to 500 °C in 50 °C steps, and from 500 °C to room temperature in 100 °C steps. After each heating step, a diffraction pattern was recorded over the angular range $9° \leqslant 2\theta \leqslant 18°$. Fig. 5 illustrates the temperature programmed X-ray powder diffraction patterns of $Pr_4B_{10}O_{21}$, showing a decomposition of the high-pressure phase into α-$Pr(BO_2)_3$ and supposable B_2O_3 at a temperature of 900 °C. At 1100 °C, a side reaction of α-$Pr(BO_2)_3$ with the quartz capillary occurs, leading to $Pr(BSiO_5)$ [41]. Despite of the metastable character of $Pr_4B_{10}O_{21}$, it is stable up to a temperature of 850 °C.

5. Conclusions

With the high-pressure synthesis of $Pr_4B_{10}O_{21}$, we were able to add a new composition to the field of rare-earth oxoborates. In accordance with the relatively mild applied pressure of 3.5 GPa, the structure consists of $[BO_3]^{3-}$ and $[BO_4]^{5-}$ groups in the ratio 1:4. The investigation of other rare-earth oxoborates, composed of $RE_4B_{10}O_{21}$ with larger and smaller rare-earth ions and the structural influence of the varying radius of the rare-earth ions, will be the subject of our future efforts.

Acknowledgments

We would like to thank Thomas Miller for collecting the single-crystal data and for the temperature programmed *in-situ* powder diffraction measurements. Special thanks go to Prof. Dr. W. Schnick (LMU München) for his continuous support of these investigations. This work was sponsored by the Deutsche Forschungsgemeinschaft (HU 966/2–2) and the European Science Foundation within the COST D30 network (D30/003/03). H. Huppertz is indebted to the Fonds der Chemischen Industrie for financial support.

References

[1] H. Huppertz, Z. Naturforsch. B 58 (2003) 257.
[2] H. Huppertz, G. Heymann, Solid State Sci. 5 (2003) 281.
[3] H. Emme, M. Weil, H. Huppertz, Z. Naturforsch. B 60 (2005) 815.
[4] H. Huppertz, B. von der Eltz, R.-D. Hoffmann, H. Piotrowski, J. Solid State Chem. 166 (2002) 203.
[5] H. Emme, H. Huppertz, Acta Crystallogr. C 60 (2004) i117.
[6] H. Emme, C. Despotopoulou, H. Huppertz, Z. Anorg. Allg. Chem. 630 (2004) 2450.
[7] G. Heymann, T. Soltner, H. Huppertz, Solid State Sci. 8 (2006) 821.
[8] J.S. Knyrim, P. Becker, D. Johrendt, H. Huppertz, Angew. Chem. Int. Ed. Engl. 45 (2006) 8239.
[9] J.S. Knyrim, F.M. Schappacher, R. Pöttgen, J. Schmedt auf der Günne, D. Johrendt, H. Huppertz, Chem. Mater. 19 (2007) 254.
[10] J.S. Knyrim, H. Huppertz, J. Solid State Chem. 180 (2007) 742.
[11] H. Huppertz, B. von der Eltz, J. Am. Chem. Soc. 124 (2002) 9376.
[12] H. Huppertz, Z. Naturforsch. B 58 (2003) 278.
[13] H. Huppertz, H. Emme, J. Phys.: Condens. Matter 16 (2004) S1283.
[14] H. Emme, H. Huppertz, Z. Anorg. Allg. Chem. 628 (2002) 2165.
[15] H. Emme, H. Huppertz, Chem. Eur. J. 9 (2003) 3623.
[16] H. Emme, H. Huppertz, Acta Crystallogr. C 61 (2005) i29.
[17] H. Huppertz, S. Altmannshofer, G. Heymann, J. Solid State Chem. 170 (2003) 320.
[18] H. Emme, H. Huppertz, Acta Crystallogr. C 61 (2005) i23.
[19] H. Emme, M. Valldor, R. Pöttgen, H. Huppertz, Chem. Mater. 17 (2005) 2707.
[20] D. Walker, M.A. Carpenter, C.M. Hitch, Am. Mineral. 75 (1990) 1020.
[21] D. Walker, Am. Mineral. 76 (1991) 1092.

[22] H. Huppertz, Z. Kristallogr. 219 (2004) 330.
[23] D.C. Rubie, Phase Transitions 68 (1999) 431.
[24] N. Kawai, S. Endo, Rev. Sci. Instrum. 8 (1970) 1178.
[25] W. Herrendorf, H. Bärnighausen, HABITUS-Program for numerical absorption correction, University of Karlsruhe/Giessen, Germany, 1993/1997.
[26] G. M. Sheldrick, SHELXS-97 and SHELXL-97, Program suite for the solution and refinement of crystal structures, University of Göttingen, Germany, 1997.
[27] J.W. Visser, J. Appl. Crystallogr. 2 (1969) 89.
[28] WinX^{POW} Software, STOE & CIE GmbH, Darmstadt, Germany, 1998.
[29] E. Zobetz, Z. Kristallogr. 191 (1990) 45.
[30] F.C. Hawthorne, P.C. Burns, J.D. Grice, In: E.S. Grew, L.M. Anovitz (Eds.), Boron: Mineralogy, Petrology and Geochemistry, vol. 33, second ed., Mineralogical Society of America, Washington, 1996, pp. 41.
[31] E. Zobetz, Z. Kristallogr. 160 (1982) 81.
[32] C. Sieke, T. Nikelski, Th. Schleid, Z. Anorg. Allg. Chem. 628 (2002) 819.
[33] I.D. Brown, D. Altermatt, Acta Crystallogr. B 41 (1985) 244.
[34] N.E. Brese, M. O'Keeffe, Acta Crystallogr. B 47 (1991) 192.
[35] M. Ren, J.H. Lin, Y. Dong, L.Q. Yang, M.Z. Su, L.P. You, Chem. Mater. 11 (1999) 1576.
[36] J.P. Laperches, P. Tarte, Spectrochim. Acta 22 (1966) 1201.
[37] G. Blasse, G.P.M. van den Heuvel, Phys. Status Solidi 19 (1973) 111.
[38] W.C. Steele, J.C. Decius, J. Chem. Phys. 25 (1956) 1184.
[39] R. Böhlhoff, H.U. Bambauer, W. Hoffmann, Z. Kristallogr. 133 (1971) 386.
[40] K. Machida, H. Hata, K. Okuno, G. Adachi, J. Shiokawa, J. Inorg. Nucl. Chem. 41 (1979) 1425.
[41] I.Y. Nekrasov, R.A. Nekrasova, Dokl. Akad. Nauk SSSR 201 (1971) 179.